Preprints of the 21st IFAC World Congress (Virtual)
Berlin, Germany, July 12-17, 2020

Simulation of RF Noise Propagation to Relativistic Electron Beam Properties in a Linear Accelerator

Andrei Maalberg [*,**] **Michael Kuntzsch** [*] **Eduard Petlenkov** [**]

[*] *Helmholtz-Zentrum Dresden-Rossendorf, 01328 Dresden, Germany (e-mail: {a.maalberg, m.kuntzsch}@hzdr.de)*
[**] *Department of Computer Systems, Tallinn University of Technology, 19086 Tallinn, Estonia (e-mail: {andrei.maalberg, eduard.petlenkov}@taltech.ee)*

Abstract: The control system of the superconducting electron linear accelerator ELBE is planned to be upgraded by a beam-based feedback. As the design of the feedback algorithm enters its preliminary stage, the problem of analyzing the contribution of various disturbances to the development of the electron beam instabilities becomes highly relevant. In this paper we exploit the radio frequency (RF) phase and amplitude noise data measured at ELBE to create a behavioral model in Simulink. By modeling the interaction between a RF electromagnetic field and an electron bunch traversing a bunch compressor we analyze how the addition of RF noise impacts the electron beam properties, such as energy, duration and arrival time.

Keywords: Electron Linear Accelerator; Bunch Compression; RF Noise; Simulink Model

1. INTRODUCTION

Particle accelerators are one of the most valuable tools to conduct large-scale research nowadays. The opportunities provided by such tools are used in a number of research centers around the world, including the one located in Dresden, Germany—Helmholtz-Zentrum Dresden-Rossendorf, or HZDR. An Electron Linear accelerator for beams with high Brilliance and low Emittance (ELBE) is operated at HZDR in continuous wave (CW) mode providing a versatile light source for scientific experiments. Represented by a beam of ultra-short photon pulses this light source is generated using accelerated electrons. By illustrating a fraction of the schematic layout of ELBE Figure 1 presents the path from the creation of electrons to their acceleration to the generation of photons.

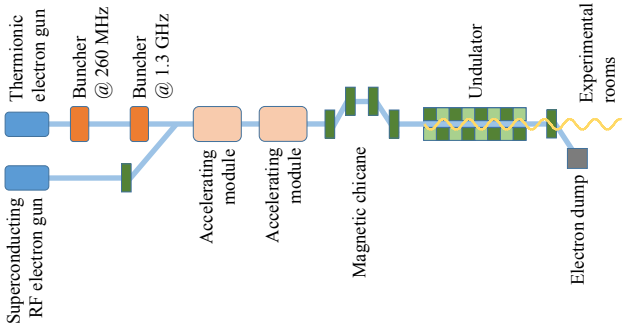

Fig. 1. Schematic layout of ELBE

In order to achieve acceptable quality of the generated photon pulses the properties of the electron beam, such as the energy, the arrival time and the electron bunch duration, must fulfill certain stability requirements. The process of stabilization is performed by controlling the amplitude and phase of the accelerating RF field, because these parameters actively participate in the beam acceleration process and thus affect the above-mentioned properties. Typically though this control scheme accounts neither for the electron beam measurements, nor other sources of instabilities, e.g. the noise contribution from the electron gun. Consequently, such control scheme has its limitations (Schmidt (2010)). A more robust way would be to control the beam properties by introducing a beam-based feedback. In this extended scheme the controller that controls its dedicated RF field—a local low-level radio frequency (LLRF) controller—takes the beam measurements into account. There exists a number of beam-based feedback designs in the field of linear accelerators (Rezaeizadeh et al. (2015); Pfeiffer (2014)), and each of them may greatly depend on the characteristics of its corresponding accelerator machine. As the existing control scheme at ELBE is planned to be upgraded by a beam-based feedback, the characteristics of this linear accelerator, including CW operation mode, superconductivity of RF cavities and high electron bunch repetition rate, need to be examined in order to have a proper understanding of the system in terms of control engineering.

The preliminary examination shows that the controlled variables, i.e. the amplitude and phase of the accelerating RF field, can be heavily constrained by the bandwidth of the corresponding RF cavity. For example, a superconducting cavity is essentially a band-pass filter with a very narrow bandwidth of a couple hundred hertz (Schilcher (1998)). Consequently, considering a bunch repetition rate in the order of 10 MHz the bunch-by-bunch control becomes practically infeasible. Furthermore, this work shows that the bandwidth of the actual disturbances that act

on the electron beam is well below 1 MHz with one of the major contributors being the RF cavity itself. Of course, the ultimate disturbance coverage is not complete without considering 1) the beam arrival time instabilities coming from the electron gun and 2) the beam-RF interactions commonly referred to as the beam loading (Garoby (1992)). Nevertheless, 1) we show that the methods developed in this work can be extended to incorporate the beam arrival time instabilities and 2) we leave the beam loading effect for our subsequent works. Therefore, we believe that by analyzing the contribution of RF cavity noise to the development of electron beam instabilities we can make the first step to designing a beam-based feedback algorithm capable of compensating these instabilities more efficiently.

This paper is organized as follows: Section 2 explores the noise data measured at ELBE. Sections 3 and 4 deal with the analytic modeling of RF noise and linear accelerator respectively. In Section 5 a Simulink model is built allowing to simulate the interaction between a RF electromagnetic field and an electron bunch. Simulation results are presented in Section 6. Finally, Section 7 concludes the paper.

2. MEASUREMENT DATA

The data demonstrated in Figure 2 was measured using a Rohde & Schwarz Phase Noise Analyzer (Feldhaus and Roth (2016)) at one of the superconducting RF (SRF) cavities installed at ELBE. This data shows the closed loop noise behavior of the accelerating RF field, and since the latter is an important region of interaction between an electron beam and an accelerator, the presented data can be exploited as first principles in order to build a simulation model that will help analyze the behavior of the beam under various RF noise conditions. Additionally, the significance of this data comes from the fact that it represents the noise behavior of a cavity under the influence of a local digital LLRF controller. This is important from the point of view of the future beam-based feedback algorithm which will have to account for these local LLRF controllers and cooperate with them.

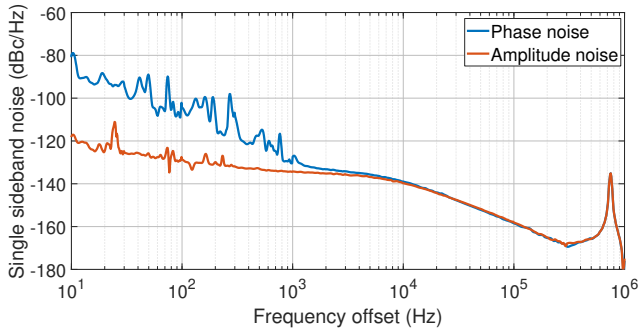

Fig. 2. Single sideband cavity noise measured at ELBE

2.1 Data Analysis

An ideal RF signal would be represented by a single spectral line. Typically, however, the spectral representation will contain a spread of spectral lines both below and above the carrier frequency. These additional spectral components, or sidebands, are caused by unwanted amplitude and phase fluctuations. According to the standard (IEEE Standard 1139-2008 (2009)), Figure 2 depicts the spectral components of both the phase and amplitude noise as

$$10\log\left(\frac{1}{2}S_\phi(f)\right), \qquad 10\log\left(\frac{1}{2}S_a(f)\right), \tag{1}$$

where $S_\phi(f)$ and $S_a(f)$ are one-sided spectral densities of the phase and amplitude fluctuations respectively.

Structurally, the phase and amplitude noise frequency data presented in Figure 2 contain two components: 1) a shape profile that decays with certain slopes as the frequency offset increases and 2) a number of spikes, or spurs, along this profile. In fact, the first one corresponds to the *random* noise component, while the second one is the result of *deterministic* noise sources.

The slopes of the random components present in the measured data can be defined by piecewise-linear approximation as shown in Table 1. Even though it is clear that in the low frequency range the power of the amplitude fluctuations is much lower than the one of the phase, in the higher frequency range the shape profiles start to coincide. This is one of the reasons not to neglect amplitude noise in the current analysis.

Table 1. Random noise slopes of measured data

Phase noise	
Frequency range	dB/dec
10 Hz – 1 kHz	–23.75
1 kHz – 10 kHz	0
10 kHz – 1 MHz	–24

Amplitude noise	
Frequency range	dB/dec
10 Hz – 100 Hz	–10
100 Hz – 10 kHz	0
10 kHz – 1 MHz	–24

The spurs of the deterministic components come from specific periodic sources, including voltage ripple at 50 Hz and vacuum pump vibrations at 10 and 24 Hz. The large spur at ca. 750 kHz corresponds to the $^8/_9\ \pi$ fundamental mode of a TESLA cavity (Vogel (2007)). Importantly, the fact that these noise sources are identifiable can later be leveraged to the advantage of the future beam-based feedback algorithm.

Finally, Figure 3 illustrates the noise of a RF signal in the time domain. Later in this paper it will become clear how these RF fluctuations can have a direct impact on an accelerated electron beam.

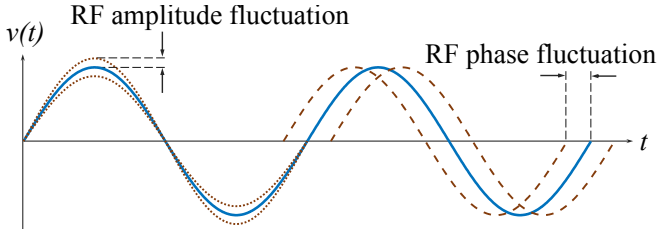

Fig. 3. RF noise in time domain

3. RF NOISE MODELING

A noisy sinusoidal oscillator waveform can be represented as (Demir and Sangiovanni-Vincentelli (1996))

$$v(t) = (A_c + \alpha(t))\cos(2\pi f_c t + \varphi(t) + \phi_0), \tag{2}$$

where A_c is the amplitude and f_c is the frequency of the carrier, ϕ_0 is the initial phase, while $\alpha(t)$ and $\varphi(t)$ are

zero-mean random processes representing the amplitude and phase noise of the oscillator waveform respectively. Therefore, by extracting the random noise definition from (2) and augmenting it with a deterministic zero-mean component we model the amplitude and phase noise as

$$A_n(t) = \alpha(t) + \sum_{i=1}^{n} A_{d_i} \sin(2\pi f_{d_i} t), \tag{3}$$

$$\phi_n(t) = \varphi(t) + \sum_{i=1}^{n} A_{d_i} \sin(2\pi f_{d_i} t), \tag{4}$$

where $A_n(t)$ and $\phi_n(t)$ are the amplitude and phase noise terms acting on the RF electromagnetic field respectively, while A_d is the amplitude and f_d is the frequency of a deterministic noise signal. From (3) and (4) it is now obvious that the RF noise profile observed in Figure 2 shall be modeled by the random processes $\alpha(t)$ and $\varphi(t)$, while the spurious content of the measured RF noise shall be the responsibility of the deterministic sine wave sums.

4. LINEAR ACCELERATOR MODELING

In this paper a linear accelerator shall be modeled in terms of a bunch compressor. Figure 4 schematically demonstrates this concept.

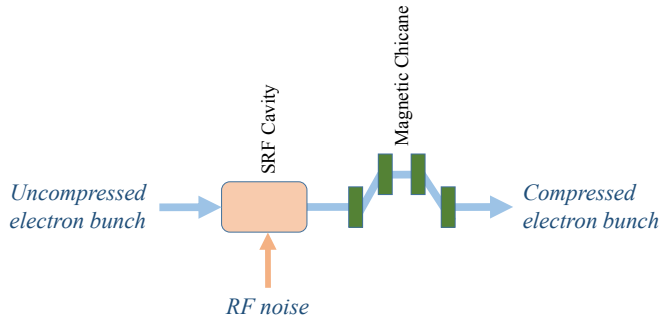

Fig. 4. Schematic of bunch compressor concept

The importance of bunch compression in this context is that the concept describes the interaction between the electron beam and important accelerator structures, namely the RF cavity and the magnetic chicane. Therefore, bunch compression provides a suitable way to analyze the propagation of RF noise to the electron beam. Before going into the modeling details though, it is important to explain why and when longitudinal electron beam dynamics can be expressed using static maps.

4.1 Usage of Static Maps

Unlike a synchrotron where the circulating particles exhibit an inherently periodic longitudinal motion—the so called synchrotron oscillation, a linear accelerator is a single-pass machine, and thus the particles exhibit little to none periodicity in their longitudinal motion (Wille (2000)). Moreover, in case of linear machines that operate with electrons, the latter require relatively low acceleration energies in order to reach the relativistic regime (Rosenzweig (2003)). In this regime the particles travel with almost the speed of light, the space charge effect that makes the particles repel each other becomes negligible, and hence the longitudinal motion inside an electron bunch becomes effectively *'frozen'*. All this leads to the fact that the longitudinal motion of relativistic electrons inside a linear accelerator can be described using static maps.

4.2 Bunch Compression

The process of bunch compression is twofold: 1) first an energy chirp is introduced into the particle distribution of an electron bunch by accelerating the latter off-crest in a RF cavity and 2) then this energy chirp is used to vary the path lengths of the particles in a magnetic chicane in order to bring the particles closer together (Chao et al. (2013)).

When an electron bunch is accelerated off-crest the particles in the head of the bunch see less RF amplitude compared to the particles arriving in the tail of the bunch. This time-energy correlation results in a certain energy distribution along the bunch—the energy chirp. Figure 5 illustrates the off-crest acceleration together with the phase space representation of the resulting energy chirp.

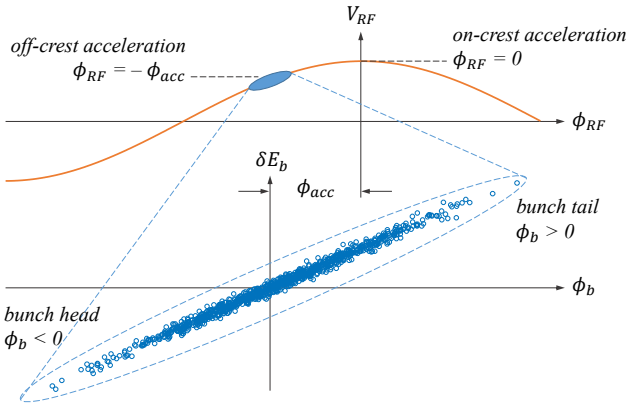

Fig. 5. RF off-crest acceleration and energy chirp

Therefore, mathematically such acceleration and, hence, the RF cavity stage of the bunch compression can be described using the following expression

$$E_f = E_i + eV\cos(\phi), \tag{5}$$

where E_f and E_i are the final and initial energies of the electron bunch particles respectively, V is the amplitude and ϕ is the phase of the RF electromagnetic field, and finally e is the electron charge. From (5) it becomes immediately clear how RF fluctuations demonstrated in Figure 3 can start propagating to the electron bunch.

The second stage of the bunch compression, i.e. the magnetic chicane, uses a static magnetic field to bend the trajectories of the electron bunch particles depending on their energy. The magnets of the chicane are arranged in such a way that the particles with a higher energy take a shorter path through the chicane, while the particles with a lower energy take a longer path. Considering that the energy chirp is imprinted such that the head of the bunch has less energy than the tail results in a situation that the delayed head lets the tail catch up with it, hence the compression of the bunch. The energy dependent path deviation is expressed mathematically as follows

$$z_f = z_i + R_{56}\frac{\Delta E}{E_0}, \tag{6}$$

where z_f and z_i are the final and initial positions of the particles in the electron bunch w.r.t. the mean position respectively, E_0 is the nominal energy of the electron bunch expected at the magnetic chicane, while ΔE is the deviation of the particle energy from this nominal energy, and finally R_{56} is a factor that translates the energy deviation into longitudinal position deviation which is a design parameter of the magnetic chicane. Considering that the energy of the electron bunch may already be disturbed by the RF fluctuations, equation (6) demonstrates how this disturbance is further mapped to longitudinal position fluctuations.

To sum up, (5) and (6) represent the static maps which can be used to model a linear accelerator for the purpose of this paper.

5. SIMULATION MODEL

Following the discussion in Sections 3 and 4 we can now start building a Simulink model as a tool to analyze how the RF noise propagates to the electron beam.

5.1 Top Level Block Diagram

The top level view of the simulation model is depicted in Figure 6. The responsibilities of the presented Simulink blocks are divided as follows

- RF Electromagnetic Field realizes the discussion of Section 3;
- Bunch Compressor contains the necessary logic to implement the linear accelerator modeling presented in Section 4;
- Electron Bunch Timing and Phase Sum will be presented in Section 5.3;
- Beam Diagnostics encapsulates the details of deriving and then plotting the resulting beam properties.

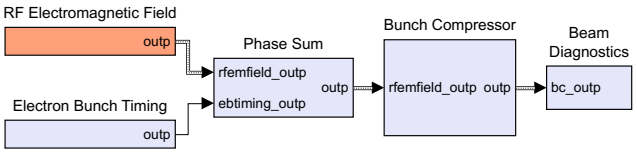

Fig. 6. Top level block diagram in Simulink

Additionally, this simulation model can be run with various parameters as shown in Table 2. Among other parameters the bunch repetition rate is of particular interest in the context of this discussion. Generally speaking, we say that an electron bunch samples the RF electromagnetic field noise, hence the bunch repetition rate is in fact the sampling frequency of this noise. Now as the main noise contribution has a bandwidth below 1 MHz, choosing a bunch repetition rate of 3.25 MHz not only conforms to the rates used at ELBE, but also respects the corresponding Nyquist frequency.

5.2 RF Electromagnetic Field

The RF electromagnetic (EM) field is modeled as a combination of the corresponding amplitude and phase parameters. Since the modeling of these parameters in the context of this paper happens to be quite similar, we start by presenting a generalized Simulink model and in the end introduce model parts that are parameter dependent.

Table 2. Parameters of simulation model

Parameter	Value	Unit
RF frequency	1.3	GHz
RF gradient	8	MV/m
RF phase	–60	degrees
Bunch repetition rate	3.25	MHz
Bunch particle number	1000	dimensionless
Bunch initial duration	3	picoseconds
Bunch initial energy	18	MeV
Bunch initial energy spread	37.2	keV
Magnetic chicane R_{56}	–110	millimeters

Based on (3) and (4) the generation of the RF electromagnetic field parameter, i.e. the amplitude or the phase, can be modeled in Simulink as depicted in Figure 7.

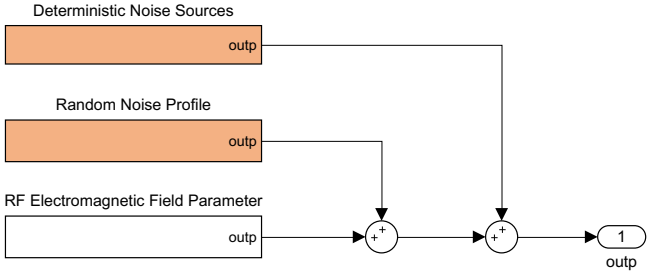

Fig. 7. Generation of RF EM field parameter in Simulink

Moreover, according to (3) and (4) we know that the deterministic noise is modeled as a sum of sine waves. Figure 8 displays a Simulink model that includes three sine wave generators for frequencies: 1) 10 Hz to denote a vacuum pump, 2) 50 Hz to describe voltage ripple and 3) 750 kHz to indicate the above-mentioned $^8/_9$ π fundamental cavity mode. These sources are represented by idealized sinusoidal waveforms with the amplitudes calculated as

$$A_i = \sqrt{\alpha 10^{\frac{M_i + \frac{N_0}{2}}{10}} w}, \tag{7}$$

where M_i is the magnitude of a spur in dBc/Hz units as observed in Figure 2, while A_i is the amplitude of the corresponding sine wave in volts, α is a dimensionless window correction factor (Harris (1978)), w is the resolution bandwidth of the spectrum analyzer in hertz, and, finally, $\frac{N_0}{2}$ is the two-sided power spectral density of a white Gaussian noise as defined in (8). In comparison, the $\frac{N_0}{2}$ constant in (7) must be specified in decibel units.

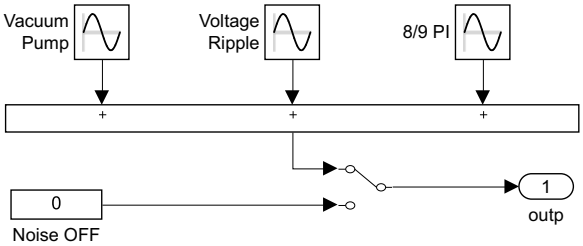

Fig. 8. Generation of deterministic RF noise in Simulink

Furthermore, from (3) and (4) we also remember that the random component, i.e. $\alpha(t)$ or $\varphi(t)$, is a zero-mean

random process that represents the corresponding amplitude and phase noise. Obviously, such definition can be modeled as a white Gaussian noise filtered according to the measured shape presented in Figure 2. Consequently, this concept can be implemented in Simulink as demonstrated in Figure 9.

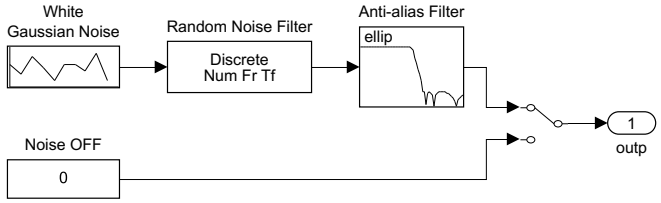

Fig. 9. Generation of random RF noise in Simulink

The variance of the white Gaussian noise is specified as (Ziemer and Tranter (2014))

$$\sigma^2 = 2\frac{N_0}{2}B, \tag{8}$$

where B is the bandwidth of the noise profile in hertz, while $\frac{N_0}{2}$ is the two-sided power spectral density of the white noise process in watts, and since we are only interested in a one-sided spectrum we double this constant. In this simulation we use variance with $\frac{N_0}{2}$ constant being equal to 1.

Regarding the random noise filter, Table 1 shows that the measured random noise shapes have regions with slopes that cannot be precisely described by the linear time-invariant (LTI) systems that adhere to the $n{\cdot}20$ dB/dec rule with $n \in \mathbb{Z}$. Still, such problems have been solved before using fractional order modeling (Heuer et al. (2014)). Therefore, we define a fractional order transfer function for the amplitude noise using FOMCON toolbox (Tepljakov et al. (2019)) as

$$W_a(s) = 1.44 \cdot 10^{-2} \frac{\left(s^{0.82} + 6.28 \cdot 10^2\right)}{\left(s^{0.75} + 62.8\right)\left(s^{1.124} + 1.8 \cdot 10^5\right)}. \tag{9}$$

Likewise, the phase noise shape filter is defined by its fractional order transfer function as

$$W_\phi(s) = 6.18 \cdot 10^{-2} \frac{\left(s^{1.05} + 1.257 \cdot 10^4\right)}{\left(s^{1.1} + 62.8\right)\left(s^{1.115} + 2.2 \cdot 10^5\right)}. \tag{10}$$

In this work both transfer functions were tuned empirically. Figures 10 and 11 show the magnitude frequency response of (9) and (10) respectively. The corresponding measured RF noise shapes are added to these Figures in order to validate the filter shapes.

5.3 Electron Bunch Timing

The arrival time of relativistic electron bunches can be related to phase in radians as

$$\phi_{bunch}(t) = t_{arr} \cdot \omega(t), \tag{11}$$

where $\omega(t)$ is the angular frequency of the arriving electron bunches, while t_{arr} is the arrival time itself. Conceptually, this electron bunch phase is very important since it directly affects the accelerating RF phase. By extending (5) this concept can be analytically expressed as

$$E_f = E_i + eV\cos\left(\phi_{RF} + \phi_{bunch}\right). \tag{12}$$

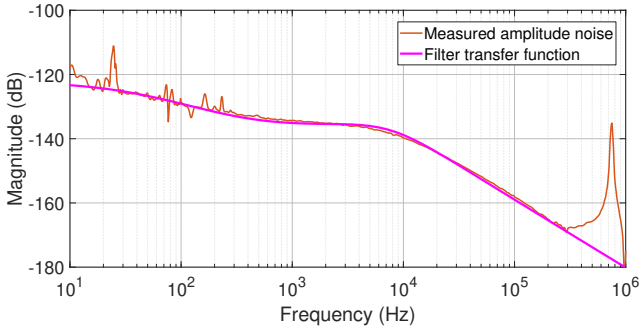

Fig. 10. Bode plot of random amplitude noise filter

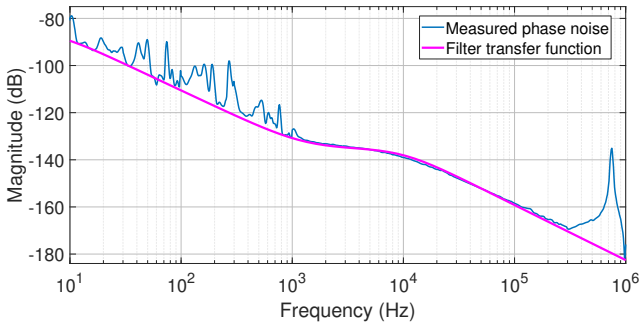

Fig. 11. Bode plot of random phase noise filter

In terms of Simulink modeling this phase sum concept is implemented in PHASE SUM block seen in Figure 6.

Now, regarding the electron bunch phase, or timing, block ELECTRON BUNCH TIMING displayed in Figure 6 models this input beam parameter as illustrated in Figure 12. In the presented block diagram we can clearly see the reuse of the methods developed in Section 5.2. Consequently, the noise placeholders allow straightforward extension of the model by beam arrival time instabilities.

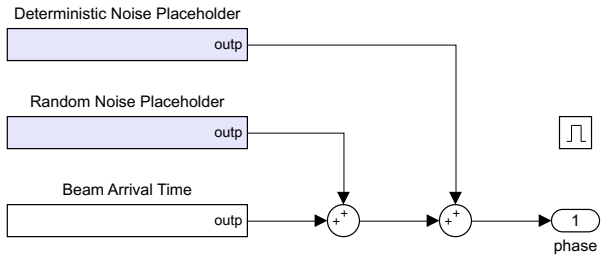

Fig. 12. Simulink model of electron bunch timing

5.4 Bunch Compressor

Modeling (5) and (6) using Simulink blocks results in a bunch compressor model demonstrated in Figure 13. While blocks RF CAVITY MAP and MAGNETIC CHICANE MAP implement the corresponding analytic expressions, block ELECTRON BUNCH GUN simply outputs an electron bunch in a phase space representation, i.e. two vectors with a Gaussian distribution: 1) for the particle longitudinal positions inside the bunch w.r.t. the mean position and 2) for the absolute energies of these particles. The size of these phase space vectors corresponds to the number of particles specified in Table 2.

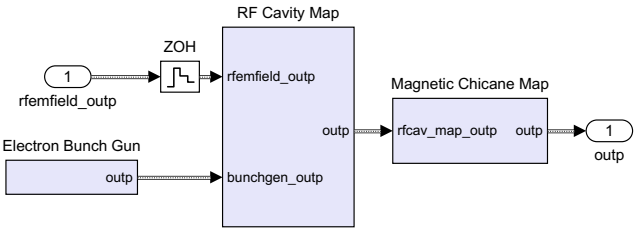

Fig. 13. Bunch compressor modeled in Simulink

Furthermore, block ZOH, i.e. zero-order hold, makes the bunch compressor model effectively discrete. The sampling frequency corresponds to the specified bunch repetition rate in Table 2. Indeed, by letting the bunch compressor model periodically sample the RF electromagnetic field with the actual bunch repetition rate we mimic how an electron bunch travels through this accelerator structure sampling potential RF disturbances along the way.

5.5 Beam Diagnostics

As stated in Section 5.4 the electron bunches emitted by Electron Bunch Gun block have phase space representation. When traversing RF Cavity and Magnetic Chicane blocks this initial electron phase space will change resulting in a final phase space which corresponds to a compressed electron bunch. Consequently, when Beam Diagnostics block receives these compressed electron bunches, the derivation of the bunch energy, arrival time and duration becomes merely a manipulation of the final phase space representation using formulae (13), (14) and (15) respectively

$$\langle E \rangle = \frac{1}{n} \sum_{i=1}^{n} E_i, \tag{13}$$

$$\langle t \rangle = \frac{1}{c} \frac{1}{n} \sum_{i=1}^{n} z_i, \tag{14}$$

$$\sigma_t = \frac{1}{c} \sqrt{\frac{1}{n-1} \sum_{i=1}^{n} (z_i - \langle z \rangle)^2}, \tag{15}$$

where E_i is the absolute energy of the i-th particle inside an electron bunch in electron-volts and $\langle E \rangle$ is the mean energy of the whole ensemble of particles; z_i is the longitudinal position of the i-th particle within an electron bunch in meters w.r.t. the mean position, c is the speed of light and $\langle t \rangle$ is the mean position converted into time in seconds; finally, σ_t is the standard deviation of the longitudinal particle positions inside the bunch converted into time in seconds.

6. SIMULATION RESULTS

The simulation model described in Section 5 produces RF noise with a frequency spectrum displayed in Figure 14. The resolution bandwidth of the spectrum analyzer was set to 1 Hz. The addition of the measured RF noise to this illustration validates the correctness of the developed RF noise shape filters. Moreover, the decibel levels of the simulated spurious content correspond to the measured ones which shows the correctness of (7). Without loss of generality the simulated spurious content is represented only by the spurs introduced in Section 5.2 plus the vacuum pump vibrations at 24 Hz for the amplitude noise.

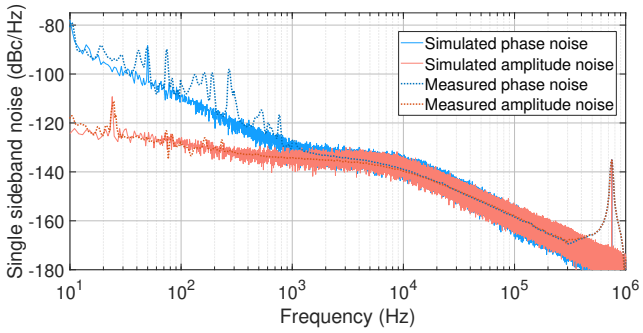

Fig. 14. Simulated RF noise frequency spectrum

Afterward, the amplitude and phase noise components were separately applied to the electron beam properties, such as energy, duration and arrival time. The resulting frequency spectra can be observed in Figures 15 and 16. The direct correspondence of these output spectra to the input one shown in Figure 14 clearly underscores the static behavior of the bunch compressor. The only detail that can change in this case is the scaling—an inherent feature of a static system. Obviously, this scaling also depends on the units of the beam properties, hence the specification of the units on the plots.

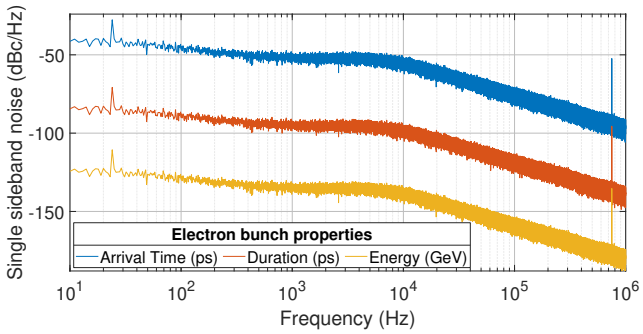

Fig. 15. RF amplitude noise applied to beam properties

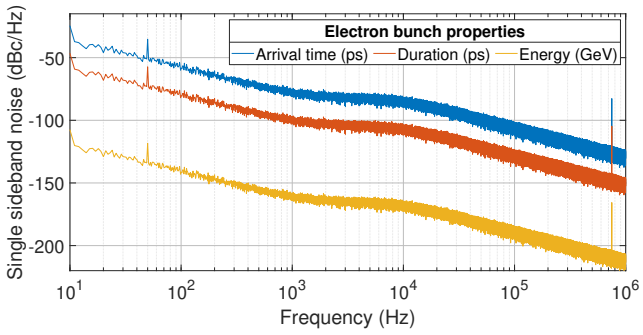

Fig. 16. RF phase noise applied to beam properties

Finally, running the simulation with both RF noise components applied to the electron beam properties produces the result presented in Figure 17. A noteworthy observation is that the energy and arrival time properties of an electron bunch seem to follow the amplitude noise dynamics, while the duration property appears to be influenced by the

phase noise dynamics. Additional sensitivity analysis may be required to explain this observation.

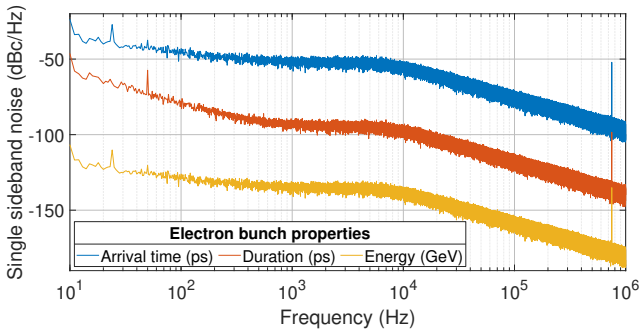

Fig. 17. RF noise applied to beam properties

7. CONCLUSIONS

A proper understanding of the contribution of RF noise to the development of electron beam instabilities is essential in order to design an efficient beam-based feedback control algorithm. Moreover, the relevance of this understanding is supported by the fact that every particle accelerator in the world, including the superconducting electron linear accelerator ELBE, is considered unique, hence no general control solution exists.

In this paper we used the RF noise data measured at one of the superconducting RF cavities installed at ELBE in order to build a Simulink model that could help analyzing the propagation of the RF noise to the electron beam properties. Using this simulation model we showed that from a control point of view an electron bunch compressor of a linear accelerator operating on relativistic particles exhibits a static behavior. Therefore, there is a direct correlation between the frequency spectra of the RF noise and the electron beam properties.

Furthermore, the presented measurement data highlighted the fact that simple LTI systems do not allow precise description of the RF phase noise shapes. Hence, fractional order modeling was used to design the noise shape filters. Admittedly, fractional order systems are appropriate candidates to describe phase noise dynamics.

As the next step we could use the insight into the RF noise frequency content to interpret the perspective beam-based feedback as a disturbance rejection control problem. By utilizing the developed RF noise filters as frequency dependent disturbance weights the control problem could be generalized to enable modern control methods, such as the $\mathcal{H}_2$ optimal control in a S/KS mixed-sensitivity design formulation. Therefore, the controller synthesis would amount to minimizing the impact of the RF disturbance on the weighted combination of the beam performance and the corresponding control effort.

8. ACKNOWLEDGMENTS

This work was supported by the Estonian Research Council grant PRG658.

REFERENCES

Chao, A.W., Mess, K.H., Tigner, M., and Zimmermann, F. (2013). *Handbook of Accelerator Physics and Engineering*. World Scientific Publishing, 2 edition.

Demir, A. and Sangiovanni-Vincentelli, A.L. (1996). Simulation and Modeling of Phase Noise in Open-Loop Oscillators. In *Proceedings of Custom Integrated Circuits Conference*, 453–456. doi:10.1109/CICC.1996.510595.

Feldhaus, G. and Roth, A. (2016). A 1 MHz to 50 GHz Direct Down-Conversion Phase Noise Analyzer with Cross-Correlation. In *2016 European Frequency and Time Forum (EFTF)*, 1–4. doi:10.1109/EFTF.2016.7477759.

Garoby, R. (1992). *Frontiers of Particle Beams: Intensity Limitations*, chapter Beam loading in RF cavities, 509–541. Springer Berlin Heidelberg. doi:10.1007/3-540-55250-2_42.

Harris, F.J. (1978). On the Use of Windows for Harmonic Analysis with the Discrete Fourier Transform. *Proceedings of the IEEE*, 66(1), 51–83. doi:10.1109/PROC.1978.10837.

Heuer, M., Lichtenberg, G., Pfeiffer, S., Schlarb, H., Schmidt, C., and Werner, H. (2014). Modeling of the Master Laser Oscillator Phase Noise for the European XFEL using Fractional Order Systems. *IFAC Proceedings Volumes*, 47(3), 9235–9240. doi:10.3182/20140824-6-ZA-1003.00775.

IEEE Standard 1139-2008 (2009). IEEE Standard Definitions of Physical Quantities for Fundamental Frequency and Time Metrology—Random Instabilities. Standard, IEEE Standards Coordinating Committee 27.

Pfeiffer, S. (2014). *Symmetric Grey Box Identification and Distributed Beam-Based Controller Design for Free-Electron Lasers*. Ph.D. thesis, Hamburg University of Technology.

Rezaeizadeh, A., Schilcher, T., and Smith, R. (2015). MPC based Supervisory Control Design for a Free Electron Laser. In *Proc. 54th IEEE Conf. Decision and Control*, 1682–1686. doi:10.1109/CDC.2015.7402452.

Rosenzweig, J.B. (2003). *Fundamentals of Beam Physics*. Oxford, UK: University Press.

Schilcher, T. (1998). *Vector Sum Control of Pulsed Accelerating Fields in Lorentz Force Detuned Superconducting Cavities*. Ph.D. thesis, Hamburg University.

Schmidt, C. (2010). *RF System Modeling and Controller Design for the European XFEL*. Ph.D. thesis, Hamburg University of Technology.

Tepljakov, A., Petlenkov, E., and Belikov, J. (2019). *Handbook of Fractional Calculus with Applications*, chapter FOMCON toolbox for modeling, design and implementation of fractional-order control systems, 211–236. De Gruyter.

Vogel, E. (2007). High gain proportional rf control stability at TESLA cavities. *Physical Review Special Topics - Accelerators and Beams*, 10. doi:10.1103/PhysRevSTAB.10.052001.

Wille, K. (2000). *The Physics of Particle Accelerators: An Introduction*. Oxford University Press.

Ziemer, R. and Tranter, W. (2014). *Principles of Communications*. Wiley Publishing, 7 edition.